

Received April 3, 2019, accepted May 9, 2019, date of publication June 10, 2019, date of current version July 18, 2019.

Digital Object Identifier 10.1109/ACCESS.2019.2922064

INVITED PAPER

MmWave Vehicular Beam Selection With Situational Awareness Using Machine Learning

YUYANG WANG^{ID1}, (Student Member, IEEE), ALDEBARO KLAUTAU^{ID2}, (Senior Member, IEEE), MÓNICA RIBERO¹, (Student Member, IEEE), ANTHONY C. K. SOONG³, (Fellow, IEEE),

AND ROBERT W. HEATH^{ID}, JR.¹, (Fellow, IEEE)

¹Department of Electrical and Computer Engineering, The University of Texas at Austin, Austin, TX 78712, USA

²Department of Electrical Engineering, Federal University of Pará (UFPA), Belém 66075-110, Brazil

³Futurewei Technologies, Plano, TX 75024, USA

Corresponding author: Robert W. Heath, Jr. (rheath@utexas.edu)

This work was supported in part by a gift from Futurewei through the UT Situation Aware Vehicular Engineering Systems (UT-SAVES), and in part by the U.S. Department of Transportation through the Data-Supported Transportation Operations and Planning (D-STOP) Tier 1 University Transportation Center.

ABSTRACT Establishing and tracking beams in millimeter-wave (mmWave) vehicular communication is a challenging task. Large antenna arrays and narrow beams introduce significant system overhead configuring the beams using exhaustive beam search. In this paper, we propose to learn the optimal beam pair index by exploiting the locations and types of the receiver vehicle and its neighboring vehicles (situational awareness), leveraging machine learning classification and past beam training data. We formulate the mmWave beam selection as a multi-class classification problem based on hand-crafted features that capture the situational awareness in different coordinates. We then provide a comprehensive comparison of the different classification models and various levels of situational awareness. Furthermore, we examine several practical issues in the implementation: localization is susceptible to inaccuracy; situational awareness at the base station (BS) can be outdated due to vehicle mobility and limited location reporting frequencies; the situational awareness may be incomplete since vehicles could be *invisible* to the BS if they are not connected. To demonstrate the scalability of the proposed beam selection solution in the large antenna array regime, we propose two solutions to recommend multiple beams and exploit an extra phase of beam sweeping among the recommended beams. The numerical results show that situational awareness-assisted beam selection using machine learning is able to provide beam prediction, with accuracy that increases with more complete knowledge of the environment.

INDEX TERMS MmWave, beam alignment, situational awareness, machine learning.

I. INTRODUCTION

With the potential for high data rates, mmWave is the most viable approach to support the massive sensor data sharing in vehicular applications [2]. MmWave communication employs large antenna arrays to provide beamforming gain and gather receive power. Unfortunately, the narrow beams of mmWave communication and the high mobility are found in the vehicular context. A large codebook has to be searched *exhaustively* to align the beam pointing angles in current beam training solutions. Optimal beam pair is then configured based on the radio frequency (RF) and multi-path signatures

measured through beam training [3]–[5]. In vehicular communication, these beam training protocols become infeasible due to the highly dynamic channels and short beam coherence time.

Fortunately, wireless cellular communication systems have access to vast data resources – yet untapped – which can make beam training more efficient. At every BS, sector, and RF channel, hundreds of pilot signals are sent between the BS and users in its coverage area to measure the propagation channel *every second*. With the same cadence, the users send feedback to the BS about the measured channel, for the BS to select transmission parameters accordingly. Remarkably, this information is leveraged only over a fraction of a second and then discarded. This “*data collection - discard*” mode in

The associate editor coordinating the review of this manuscript and approving it for publication was David W. Matolak.

the wireless industry may be explained at lower frequencies due to the presence of more propagation paths in the channel, the variability in phone handset movement, and limitations in sensing capabilities of phones.

Data-driven beam training is a promising approach for mmWave vehicular systems. MmWave channels are more *deterministic* given a certain environment geometry, compared to that of the lower frequencies. As a result, the BS can *learn* the relationship between the *geometry* of surrounding objects and the beam direction, since these objects serve as blockages or reflectors and can change directions of the beams. Also, vehicles travel along roads in predictable ways, following certain patterns, such as higher density and slower speed during rush hour. Furthermore, vehicles are equipped with sensors like satellite navigation, radars, LiDARs, cameras, etc, which can be used to localize vehicles and sense the environment [2], [6]. Connected vehicles may share their positions and sensor data, leading to a notion of shared *situational awareness*. Last, the BS is well-equipped with the capability to accommodate the needs for data-driven solutions: (a) It has access to cloud and edge computing capability, (b) it is the natural data fusion hub for data generated by various types of sensors on a vehicle, and (c) it can also monitor current transmission status and is capable of caching the useful transmission records [7], [8].

We employ ensemble learning-based random forest classification for mmWave vehicular beam prediction, which is an efficient and robust solution [9]–[11]. By averaging several independent predictors, ensemble models are able to maintain the bias of individual predictors while still decreasing variance [12], [13]. A random forest [9] aggregates multiple classification trees [14], each one trained on bootstrapped training samples. In addition, the classifier splits trees using only *partial* features randomly selected for each split. The predicted class is the majority class *voted* by the bootstrapped classification trees. Decision trees are able to capture non-linear and complicated relationship among features but are susceptible to high variance in predictions and overfitting [12]. By introducing bagging and randomness to splits, random forest suffers less from overfitting and is able to generalize better [15], [16]. A review of other machine learning classification techniques tested in this paper can be found in [17].

Recently, out-of-band information aided mmWave beam training was proposed in [2], [6], [18]–[20]. The key idea is to leverage data collected from sensors like radar or other communication systems to help reduce the beam search overhead. Location information was exploited in [21] for machine learning-based beam training. The idea was to quantize the receiver location into several *bins* and then leverage statistical learning to recommend likely beam pairs. A learning-to-rank framework was used in [22] to enhance the flexibility of the learning model for continuous receiver locations. A limitation of the work in [21] and [22] is that the proposed algorithms only considered knowledge of the target vehicle, but not the locations of the other vehicles. This makes it difficult to

predict non-line-of-sight (NLOS) links without trying many beam pairs. In [23], a simulation framework was proposed to generate vehicular channels with temporally-correlated vehicle trajectories. An initial investigation was provided to solve the mmWave beam selection problem when all vehicles' (including the neighboring vehicles) locations were incorporated in the features. In addition to beam selection, it was shown in [24] that environment information of vehicle locations could also be used to predict the beam power to further automate vehicular beam training. In [23] and [24], however, the design of the environment features was not elaborated and issues in practical implementation were not discussed.

In this paper, we leverage ensemble learning-based classification to identify the appropriate beam pair for mmWave vehicular communication. We define *situational awareness* as the *locations* and *types* of the receiver and the *neighboring vehicles*. We provide a comprehensive investigation of an efficient machine learning framework for mmWave vehicular beam selection leveraging *situational awareness*. The key contributions are summarized as follows.

- Instead of only using the receiver location as in [21] and [22], we propose to exploit a *richer* set of vehicle information to predict the optimal beam pair index and configure mmWave vehicular link. We leverage situational awareness to capture reflections and different multi-path effects in the environment, and then to filter the angular characteristics of the receivers. Although regression could be used for predicting the exact angles, IEEE 802.11 ad and 5G NR only transmit and collect a limited number of fixed beam pairs. Along these lines, machine learning provides a framework to formulate beam selection as a classification problem. In particular, we formulate mmWave vehicular beam selection as a multi-class classification problem. We leverage random forest [9], an ensemble learning method that provides an efficient and robust approach for different classification problems [10], [11].
- We encode the situational awareness into different properly ordered hand-crafted features in Cartesian coordinates, polar coordinates and occupancy grids. Vehicles report their real-time locations regularly to the BS. Once the receiver initiates a beam training request, the BS constructs a *bird's-eye view* map of the current environment based on the vehicles' report of locations. The BS then filters and organizes the locations/types of the receiver and the neighboring vehicles, and formulates the situational awareness for the receiver. The database saves the beam measurement results along with the corresponding situational awareness for offline learning.
- We model and evaluate noisy features in practical implementations. Location information might be imperfect due to the location reporting delay or the localization inaccuracy of sensors. Also, the situational awareness could be *incomplete*, since some vehicles might be *invisible* to the BS if they are not connected.

- Instead of relying on single-label classification to identify the optimal beam, we provide several mechanisms to demonstrate the scalability and generalization of beam selection for large antenna arrays, at the cost of beam training among a small number of beam pairs. The system builds the solutions upon recommending a set of *candidate beams* based on situational awareness. The BS and the receiver conduct beam training within the smaller beam search space to identify the optimal beam pair. We propose to leverage the estimated probability distribution of beams to recommend the beams. Multi-label classification serves as another option which selects the *top* beams based on beam reference signal received power (RSRP).

The rest of the paper is organized as follows. Beam selection is formulated as a classification problem in Section II. The problem is motivated in Section II-A, which demonstrates the potential of applying situational awareness to predict the optimal beam. The system model is explained in Sections II-B and II-C, including the simulation setup and the ray tracing based channel modeling. Hand-crafted features are *encoded* in Section II-D and the features are ordered for concatenation in Section II-E. In Section III, realistic issues of inaccurate or missing locations in situational awareness are discussed and modeled. An overview of solutions to generalize the beam selection solution for large antenna arrays is provided in Section IV. Numerical results are demonstrated in Section V. The final conclusions are drawn in Section VI.

In this paper, all matrices are represented by large bold letters while the vectors are represented by small bold letters. Conjugate transpose of a matrix is indicated by $(\cdot)^*$, transpose of a matrix is represented as $(\cdot)^T$, the Kronecker product is denoted as \otimes , the ceiling function is denoted as $\lceil \cdot \rceil$, and the cross product of two sets is \times .

II. SYSTEM SETUP AND PROBLEM FORMULATION

In this section, we propose to learn the optimal beam pair index from situational awareness and the past beam training data using multi-class classification. We first motivate the use of situational awareness in our problem. We then discuss the data collection, the channel modeling and the feature design. We leverage an offline learning framework and establish our dataset using ray tracing simulation in an urban mmWave vehicle-to-infrastructure (V2I) network.

A. SITUATIONAL AWARENESS

BSs, also called road-side units (RSUs), are envisioned to be deployed at a relatively low height in the urban canyons (generally collocated with the lamp due to the high density of mmWave infrastructures). With vehicle mobility and the existence of a large number of vehicles with different sizes (e.g., high trucks, ambulances, SUVs, and small cars), the line-of-sight (LOS) path to the receiver might suffer from blockage, for example by a large truck, as shown in Fig. 1.

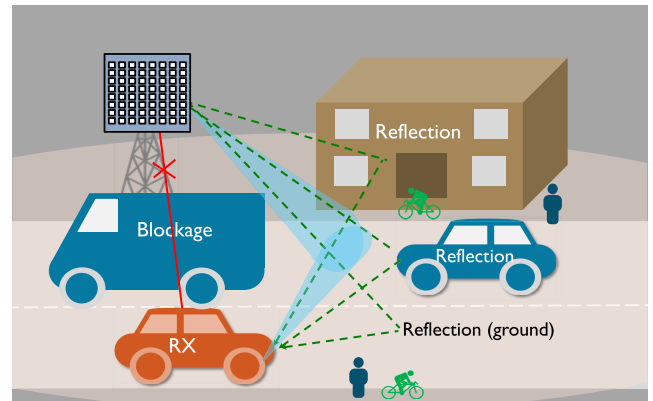


FIGURE 1. An illustration of the multiple paths of a vehicular channel in the urban canyon. The receiver is demonstrated as a red sedan. The LOS path (represented as the red line) could potentially be blocked by a large vehicle such as a truck (shown in the figure as a blue truck). The green dashed lines indicate potential reflections. In case of blockage, the alternating paths are possible due to the reflections on the buildings, on the reflecting vehicle (blue sedan), and on the ground.

Various objects in the environment can serve as reflectors for NLOS paths. Among the different types of reflecting objects, buildings, ground or other roadside construction are static, while mobile reflectors include vehicles, bicyclists, and pedestrians. In our work, we neglect the impact of pedestrians and bicyclists due to their *low height* and location at the roadway edge. Since metallic surfaces are good reflectors while they are difficult to penetrate through, vehicle is one of the primary *mobile* factors that could affect the vehicular channels [25], [26]. Thanks to the similarity of vehicle sizes, the regularity of the vehicle motion and the lane deployment, it is possible to keep track of vehicle locations and characterize the shapes and types. We define the situational awareness as knowledge of the receiver and its neighboring vehicles' locations and types.

MmWave beam are configured based on multi-path channels, which can be captured by the geometry of objects in the environment. Vehicles are the primary source of blockages and reflections for the vehicular channels. Due to the consistent antenna placement on the vehicles, vehicles' locations, shapes and sizes can determine the directions and the strengths of the paths. Hence, within the same vehicular physical environments (urban canyon, urban intersections, rural roads, etc), there exists some certain function that maps the situational awareness to the optimal beam direction. In this paper, we investigate a simple scenario, with vehicles on a two-lane straight urban street. We propose to learn the optimal beam pair index by leveraging all vehicles' *locations* and *types*, which comprise the *situational awareness* at the BS. It should be noted, however, the proposed solutions can be extended to other vehicular environments as well. Situational awareness is available in automated driving and can be obtained from sensors deployed at connected vehicles, such as GPS, radar, LiDARs, etc. In this paper, we leverage offline learning since we are primarily targeting at revealing the relationship between the situational awareness and the

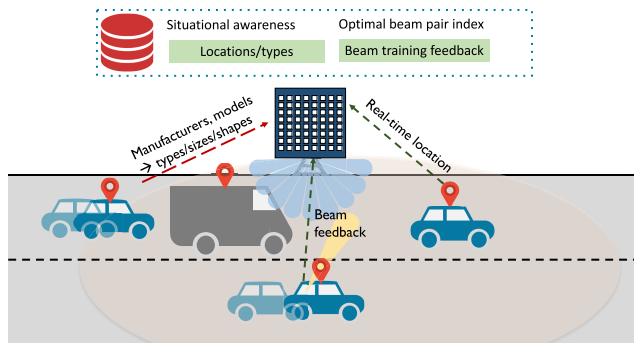


FIGURE 2. An illustration of the communication between BS and vehicles to establish the dataset. The vehicle sends its manufacturer and model information to the BS after it gets connected in the cell, which can further be translated to the information of its types, sizes and shapes. Meanwhile, the BS and vehicle conduct beam training and the optimal beam pair index is fed back to the BS. Vehicle keeps tracking and updating its real-time location to the BS. After obtaining the information of all vehicles, the BS constructs a bird's-eye view map of the vehicles in the current urban canyon and formulates the situational awareness for each vehicle, which is saved as features in the dataset. The optimal beam pair index corresponding to the situational awareness in each data sample is then used as the label for the classification.

vehicle's optimal beam pair index. The model, however, can be extended to online learning as well [23], [27], and is a topic of future work.

Fig. 2 provides a brief illustration of communication between the BS and the receiver to establish the dataset. We assume a *non-standalone* network, where a system with low frequency such as LTE or dedicated short-range communication (DSRC) coexists with mmWave. When a vehicle enters the coverage range of the BS, it detects the network and gets connected to the cell. During this process, some basic information about the vehicle, such as its manufacturer and model will be delivered to the BS, to determine its size and type. The size of vehicles can be represented by continuous values of length, height, width. The type of vehicles, such as truck, SUV, or sedan can be indicated by categorical variables. After the vehicle enters the cell, a beam training request is initiated by the vehicle. Beam sweeping is conducted between the BS and the vehicle. Beam RSRPs are measured by the vehicle and subsequently sent back and stored at the BS. The vehicle location, or in future work its trajectory, is fed back to the BS regularly. The location update frequency could either be synchronized or unsynchronized with that of the beam training request. The impact of feedback will be discussed in Section III-B.

Traditional beam selection solution involves testing candidate transmit and receive beam pairs to find the one that is likely to give the highest beam RSRP. To avoid such exhaustive search, we formulate beam selection as a *multi-class classification* problem, where features are extracted from situational awareness and the label is the categorical variable of the optimal beam pair index. It should be noted that the situational awareness is available at the BS, and all the learning and prediction are implemented at the BS. In Section II-B - II-E, we discuss the details of data collection,



FIGURE 3. Illustration of the deployment of ray tracing simulation. Small cars and trucks are randomly dropped in the two lanes of the urban canyon. Receivers are mounted on the top center of the small cars, and the BS is denoted by the green box. The figure displays the five strongest paths of the channel for a NLOS receiver. It is shown that multiple reflections happen on the buildings and the vehicles.

channel modeling, and how to encode vehicle locations and types into appropriate formats of features.

B. DATA COLLECTION FOR VALIDATION

Since there is no testbed available for mmWave V2I communication, we use a ray tracing simulator to collect data for the learning. Ray tracing is an approach to compute the propagation paths between the transmitter and receiver, given a CAD model of environment with predefined surface material properties [28]. Both industry and academia have used ray tracing for channel modeling and site-specific propagation prediction [29]–[32]. We use a commercial ray tracing simulator called Wireless Insite [33]. To validate the effectiveness of situational awareness in assisting mmWave beam selection, we consider a simple scenario with a two-lane straight street in an urban canyon shown in Fig. 3. The proposed beam selection solution can be tested and generalized by running ray-tracing simulation and collecting data in other vehicular environments as well.

The buildings are modeled by cuboids with a concrete exterior, located on both road sides with random sizes. The simulation includes two types of vehicles: high trucks, with $length, width, height = \{T_l, T_w, T_h\}$, and low cars (e.g., sedans) of size $\{C_l, C_w, C_h\}$. For simplicity, all the vehicles are modeled as cuboids with metal exteriors. In each simulation, the type of vehicle (truck and car) is determined by a Bernoulli random variable with a predefined probability. The distance between adjacent vehicles is modeled by an *Erlang distribution* with parameter (k_{erl}, θ_{erl}) to form a *sequence* of vehicles on both lanes [21], [34], [35]. The length of the simulated street is $L_{street} = 120$ m. In each of the simulation snapshot, receivers are mounted on top of only the low vehicles. The trucks are free of blockage and therefore the beam is LOS, and do not require machine learning prediction. The data and codes can be found in [36].

C. CHANNEL MODEL

Ray tracing is used to compute the top L_p strongest paths between the transmitter and the receiver, considering the effects of reflection, transmission, and diffraction. For NLOS receivers at mmWave, the strongest ray is generally determined by the first-order reflection. The ray tracing simulation formats the output angles in *spherical coordinates*, with the origin located at the transmitting antenna dipole. We take the $L_p = 25$ strongest rays from the given configurations of environment (vehicles, urban canyon, etc) and transceivers. Each path includes: (1) arrival azimuth angle ϕ^A , (2) arrival elevation angle θ^A , (3) departure azimuth angle ϕ^D , (4) departure elevation angle θ^D , (5) path gain α , (6) phase shift ω , and (7) time-of-arrival τ . We use the parameters in (1) - (7) to calculate a multi-input-multi-output (MIMO) channel impulse response [37]. Denoting the number of transmit antenna as N_t and that of receive antenna as N_r , the pulse-shaping filter as $g(\cdot)$, the steering vectors as $\mathbf{a}_t(\cdot)$ and $\mathbf{a}_r(\cdot)$, and the sampling period as T , the wideband channel $\mathbf{H}[n]$ with L_c taps is [21]

$$\begin{aligned} \mathbf{H}[n] &= \sqrt{N_t N_r} \\ &\times \sum_{\ell=0}^{L_p-1} g(nT - \tau_\ell) \mathbf{a}_r(\phi_\ell^A, \theta_\ell^A) \mathbf{a}_t^*(\phi_\ell^D, \theta_\ell^D) \alpha_\ell e^{j\omega_\ell}, \\ 0 \leq n &\leq L_c - 1. \end{aligned} \quad (1)$$

Due to the dense deployment of BSs and the short BS-vehicle distance for mmWave V2I, channels are susceptible to the change of heights and the elevation spread of departure/arrival angles [38]. To control transmit and receive beams in both the azimuth and elevation domains, we assume that both the transmitter and the receiver apply uniform planar arrays (UPA). The UPA at the transmitter faces towards the street. For the receiver, the UPA is mounted on top of the vehicle and faces upwards. The size of UPAs is denoted as $N_t = N_r = N_y \times N_x$, where N_y is the number of antenna vertically and N_x is the antenna number horizontally. Beam training is performed based on search for the transmitting beamforming and receiving combining vectors from a codebook. We use two-dimensional (2D) DFT codebooks \mathcal{W} and \mathcal{F} for the precoder and combiner, where each element of \mathcal{W} and \mathcal{F} is one beam codeword. Defining a DFT matrix \mathbf{W}_x of size $N_x \times N_x$ and \mathbf{W}_y of size $N_y \times N_y$, the i -th beam codeword in the beam codebook \mathcal{W} and \mathcal{F} is $\mathcal{W}\{i\} = \mathcal{F}\{i\} = [\mathbf{W}_x \otimes \mathbf{W}_y]_{:,i}$. Other codebooks can be used and may give higher performance if carefully designed.

A brute force approach to beam selection proceeds as follows. There are in total $N_B = N_t N_r$ different beam pairs in the dataset. For the i -th beam pair, $(\mathbf{w}_i, \mathbf{f}_i) \in \mathcal{W} \times \mathcal{F}$, $i \in \{1, 2, \dots, N_B\}$, the normalized received power p_i is

$$p_i = \sum_{n=0}^{L_c-1} |\mathbf{w}_i^* \mathbf{H}[n] \mathbf{f}_i|^2. \quad (2)$$

Stacking the received power of all beams calculated from (2), the received power vector \mathbf{p} is

$$\mathbf{p} = [p_1, p_2, \dots, p_{N_B}], \quad (3)$$

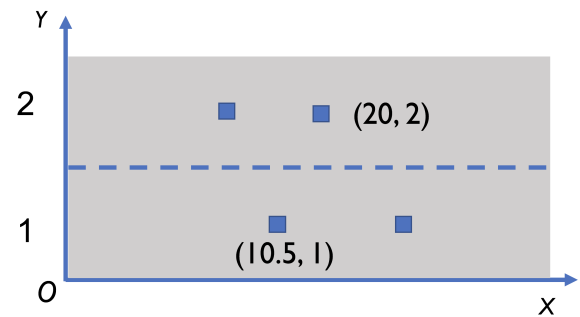


FIGURE 4. Illustration for encoding the environment with Cartesian coordinates. The origin lies at the left bottom of the simulation area. Each vehicle location is encoded as (*horizontal location, lane index*).

where N_B is the number of beam pairs in the beam codebook. Furthermore, we have

$$s = \arg \max \mathbf{p}, \quad (4)$$

and the optimal beam pair index s is obtained.

D. ENCODING VEHICLE LOCATION

The BS collects vehicle locations at fixed time intervals. To translate the raw data collected from sensors into the feature format that is suitable for our learning model, we propose the following solutions to encode the location. We evaluate the performance metrics of each encoding solution in the simulations.

1) CARTESIAN COORDINATES

The first approach is to encode locations in Cartesian coordinates, as shown in Fig. 4. The vehicles are assumed to be traveling in the center of each lane. Hence, a categorical variable is enough to represent the lane index for a vehicle. Each vehicle's location is represented by (*horizontal location, lane index*), where the horizontal location is the coordinate of the vehicle's *center* along the x coordinate. In our work, the origin of the Cartesian coordinates is set at the left bottom of the simulation area.

2) POLAR COORDINATES

Beam training with a codebook of pointing beams is essentially a problem of finding the strongest path direction in the channel. In LOS links, for example, polar coordinates (or spherical coordinates) give an exact angle-of-arrival (AoA) and angle-of-departure (AoD). As a result, polar coordinates and spherical coordinates, are a natural means to encode locations. In polar and spherical coordinates, the origin is set at the center of the receiver, as shown in Fig. 5. Each vehicle or BS's location is represented by (*distance to the origin, polar angle*), relative to the receiver. Spherical coordinates include the *elevation angle* in the three-dimensional (3D) space to incorporate the heights of different vehicles. In the spherical coordinates, each vehicle location is represented as (*distance to the origin, azimuth angle, elevation angle*).

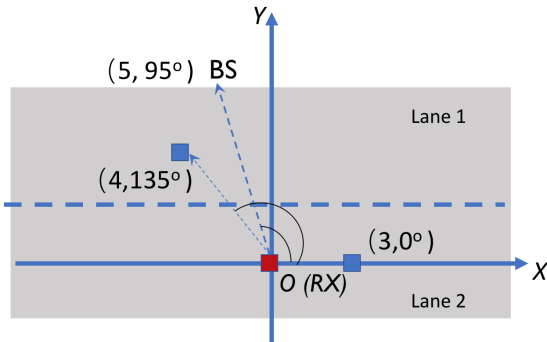


FIGURE 5. Illustration for encoding the environment with polar coordinates. The origin lies at the receiver. The *polar angle* is defined as the angle between the direction of vehicle (or BS) relative to the receiver and the x axis. Vehicle location is encoded as (*distance to the origin, polar angle*) relative to the receiver.

3) OCCUPANCY GRID

An alternative to represent the coordinates is to create an image in either 2D or 3D *occupancy grids*. For example, in the 2D case, the idea is to quantize the area into regular-sized occupancy grids with a certain *granularity* d_x . The grid granularity is quantified by the distance between the center of horizontally adjacent grids. Assuming the size of the simulation area is D_x , the grids can be represented by a matrix \mathbf{G} with a size of $2 \times \lceil \frac{D_x}{d_x} \rceil$. There are *three* types of vehicles: *neighboring trucks*, *neighboring cars*, and the *receiver car*. An illustration is provided in Fig. 6. If there is no vehicle inside the g -th grid of the ℓ -th lane ($\ell = 1, 2$), we indicate the value $\mathbf{G}[\ell, g] = 0$; if part of the truck lies inside the grid, $\mathbf{G}[\ell, g] = 1$; if part of a car (excluding the receiver) is in the grid, $\mathbf{G}[\ell, g] = 2$; if the receiver lies inside the grid, $\mathbf{G}[\ell, g] = 3$. The categorical variables 1, 2, 3, 0, are further one-hot encoded as 1000, 0100, 0010 and 0001. The occupancy grid can also be expanded into a 3D space, which is quantized into cuboids based on the pre-defined granularities. Denoting the height of the area as D_z and its granularity as d_z , the grid can be represented a matrix of size $2 \times \lceil \frac{D_x}{d_x} \rceil \times \lceil \frac{D_z}{d_z} \rceil$, where each entry characterizes the type of the vehicle that occupies the corresponding grid. The grid matrix \mathbf{G} can be kept as its original format to preserve spatial correlation and extract the patterns for example with a convolutional layer. It can also be flattened into a vector.

Similar to images composed of pixels, the grid-type features have more flexibility to manipulate, since they can encode almost any arbitrary urban canyons into images. Also, learning algorithms could work efficiently with image type features. The occupancy grid, however, encodes the locations and types in a *lossy* way due to the quantization. A higher quantization *resolution* leads to a larger dimension of features and heavier computational costs, while a low resolution cannot provide accurate characterization of the vehicle locations.

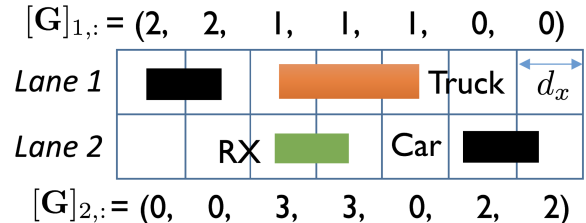


FIGURE 6. Illustration for encoding the environment in 2D regular-sized occupancy grids. Along the x-axis direction, the area of two lanes is quantized to grids of the same size. The value of the grid is determined by the type of the vehicle (or blank space) that occupies the grid. The value of the grid is denoted as 0, 1, 2, 3, respectively for the blank space, neighboring truck, neighboring car, and the receiver.

E. ORDERING THE LOCATION FEATURES

Features extracted from the physical environment need to be properly organized and integrated [39]. In our problem, vehicles are treated as individual objects and their locations are concatenated to form the feature vector with situational awareness. In the Cartesian and polar coordinates, with multiple vehicles, it still remains a challenge how to *order* all vehicles properly for feature concatenation. A good feature organization and concatenation will allow feature dimension reduction by discarding less important vehicle locations. It should be noted that occupancy grids encoding does not have an ordering problem, but does have a resolution and feature dimension tradeoff.

Neighboring vehicles could have different impacts on the receiver channel, based on their relative distance to the receiver, the type of the vehicle, or the lane they are located on. Intuitively, a vehicle close to the receiver has a higher chance of affecting beam direction than a vehicle that is located far away. Also, a vehicle in the lane closer to the BS is more likely to block the receiver on the other lane. Large trucks are more likely to block the LOS link and serve as a reflector for a path, while a small car might contribute little to the reflections. Hence, we leverage two different ordering schemes for the vehicles.

1) Natural ordering of cars and trucks

In this case, the vehicles are ordered from the left to the right in the first then the second lane. We denote \mathbf{r} as the location of the receiver (in Cartesian coordinates) or the location of the BS (in polar coordinates). The location of *all vehicles (trucks or cars) from left to right (without the receiver in Cartesian coordinates)* on the ℓ -th lane are represented as \mathbf{v}_ℓ , $\ell = 1, 2$. The feature vector \mathbf{f} is represented as

$$\mathbf{f} = [\mathbf{r}; \mathbf{v}_1; \mathbf{v}_2], \quad (5)$$

where \mathbf{v}_ℓ , $\ell = 1, 2$ includes locations of cars and trucks, which are differentiated by an one-hot encoded categorical variable, 10 or 01. For example, a car in the first lane will be represented as [horizontal distance, lane index, 10] in Cartesian coordinates.

2) ORDERED LOCATION FEATURES

Vehicle locations in the situational awareness need to be ordered when concatenated. Vehicles can be ordered based on the relative distance of the vehicle to the receiver, the type, and the lane of the vehicle. We denote the *ordered* locations of trucks on the ℓ -th lane as $\vec{\mathbf{t}}_\ell$, and those of cars as $\vec{\mathbf{c}}_\ell$. Features with ordered vehicles $\vec{\mathbf{f}}$ for each data sample can be written as

$$\vec{\mathbf{f}} = [\mathbf{r}; \vec{\mathbf{t}}_1; \vec{\mathbf{t}}_2; \vec{\mathbf{c}}_1; \vec{\mathbf{c}}_2]. \quad (6)$$

For the trucks in the first lane, we denote the horizontal location of all the trucks along the x -axis in the first lane as $[x_1, x_2, \dots, x_n]$, where n is the number of trucks in the first lane. The receiver horizontal location is x_{RX} . The relative distance of the trucks to the receiver is calculated as $d_i = |x_i - x_{RX}|$. Restricting the total number of the trucks included in the feature on each lane as N_{truck} , the locations of the trucks in the first lane $\vec{\mathbf{t}}_1$ is

$$\vec{\mathbf{t}}_1 = [x_{i_1}, x_{i_2}, \dots, x_{i_{N_{truck}}}]^T, \\ |d_{i_1}| < |d_{i_2}| < \dots < |d_{i_{N_{truck}}}|. \quad (7)$$

A fixed number of vehicles is required in the feature, for the purpose of making dimensions of features consistent under different deployment scenarios. If the number of trucks $n > N_{truck}$, the feature *deletes* the locations of the *farthest* $n - N_{truck}$ trucks from the receiver; otherwise, the feature adds in $N_{truck} - n$ *virtual* trucks that are lying very far away, where $x = \infty$ (we choose $x = 10^4$ here). Similarly, $\vec{\mathbf{t}}_2, \vec{\mathbf{c}}_1, \vec{\mathbf{c}}_2$ follow the same ordering rules as $\vec{\mathbf{t}}_1$.

Properly ordered vehicles enable consistent meanings along the different feature dimensions and avoid potential confusion for the learning model.

III. PRACTICAL IMPLEMENTATION

In practice, situational awareness could be inaccurate or incomplete. For example, location has error that depends on the localization technologies and the environment. Information may be outdated due to the limited location update frequencies. Situational awareness may also be missing due to unconnected vehicles. In this section, we describe how each of these issues may be incorporated to evaluate the system robustness.

A. LOCALIZATION INACCURACY

Location information may be obtained from different sensors, like GPS, radar, LiDARs. Each sensor has its own error model. For example, for GPS, the location error depends on the satellite geometry, blockage, atmospheric conditions, and the specific locations for GPS [40]. We model the localization error along both coordinates (x coordinate along the lane direction, and y coordinate perpendicular to the lane direction) by a location-independent *Gaussian distribution* $\mathcal{N}(0, \sigma^2)$. Furthermore, we assume that the location errors along the x and y -axes are independent. Along the horizontal direction, the localization error is directly added to

the actual vehicle location. On the y -axis, the location is added by the localization error and then *quantized* to the lane index. The effect of localization inaccuracy along the y -axis might lead to a different lane index of the vehicle and therefore a wrong feature vector. Consistently, the localization inaccuracy will be modeled in both the training and testing datasets.

B. LOCATION UPDATING FREQUENCY

Infrequent location updates introduce errors to the situational awareness due to vehicle mobility. In a connected vehicle scenario, vehicles report their locations to the BS every T_{loc} time for automate navigation purposes, while the beam training request might happen at a different interval T_{bt} . The errors in the dataset due to the outdated locations include:

(a) *Testing data*: Locations of the vehicles could become outdated due to vehicles' mobility. In the prediction phase, for example, a vehicle initiates a beam request at any time t , but might receive an *outdated* predicted beam index based on an *old* situational awareness. To match the beam training request and guarantee a low level of vehicle location errors, vehicles may have to report locations to the BS more frequently;

(b) *Training data*: In data collection, the BS receives the regular location updates and the beam feedback from the vehicle. When $T_{loc} \neq T_{bt}$, the time when beam training happens does not match that when the location is updated. The collected beam measurement is therefore inconsistent with its corresponding situational awareness, which introduces error to the training data.

We consider two mechanisms with *synchronized* and *unsynchronized* feedback, which are illustrated in Fig. 7. When $T_{loc} = T_{bt}$, there is *synchronized feedback*, while otherwise, the feedback is *unsynchronized*. At starting time t_0 , for example, the velocity of a certain vehicle is v_0 , and the acceleration is a_0 . Assuming the acceleration is *non-zero* (i.e., the vehicle is either *accelerating* or *decelerating*), and remains stable during the time interval $t_0 < t < t_0 + T_{loc}$, the location error at time t can be approximated by $x_\epsilon(t) = v_0(t - t_0) + \frac{1}{2}a_0(t - t_0)^2$. We analyze the *worst case* of outdated locations, which assumes all vehicle locations are outdated for a *maximum* of T_{loc} time, i.e., the location error equals $x_\epsilon(t_0 + T_{loc}) = v_0T_{loc} + \frac{1}{2}a_0T_{loc}^2$. We then *subtract* the error from the real location of vehicles to calculate the *outdated* location. To evaluate the effects of synchronized and unsynchronized feedback, we model the velocity and the acceleration rate as *truncated Gaussian distribution* due to practical constraints of speed limit and vehicle performance [41], [42]. For the velocity, the mean is defined as the average velocity \bar{v} m/s and the standard deviation is σ_v m/s. The mean and the standard deviation for the acceleration are respectively \bar{a} m/s² and σ_a m/s². The Gaussian distribution is then *truncated* by the upper and lower bounds for the velocities and accelerations.

To minimize the effects of the vehicle mobility on the location error, one alternative is to *pack* more information

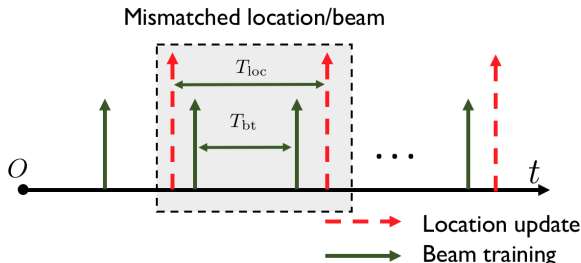


FIGURE 7. An illustration of the case with *unsynchronized* beam feedback and location update. We denote the fixed interval for location update as T_{loc} , and that of beam training (and beam feedback) as T_{bt} . When $T_{loc} = T_{bt}$, the collected data of location (situational awareness) and beam information is always *synchronized*. Beam measurement result is an exact match with the current situational awareness. When $T_{loc} \neq T_{bt}$, the *unsynchronized* location update and beam feedback leads to mismatch of the situational awareness (feature) and optimal beam pair index (label). The mismatch leads to errors in the training data.

in the feedback from vehicles to BS. Connected vehicles, by DSRC for example, are built around the SAE protocol J2735 basic safety message (BSM), which incorporates not only location, but also velocity, acceleration, and other trajectories information [43]–[45]. The BSM is broadcasted every 100 ms in SAE protocol [46]. As long as the acceleration remains stable during this interval, the BS is able to calculate the exact location error $x_e(t)$ and keep track of the vehicle location based on *equations of motion* and previous state of *mobility* parameters [47], [48]. It should also be noted that exhaustive beam search, most of the time, cannot capture the instantaneous beam changes, since the beam training only happens at fixed time slots $t = T_{bt}, 2 T_{bt}, \dots$. The proposed model, however, is flexible enough to predict any potential changes of beams, since knowledge of mobility parameters at the BS (velocity, acceleration) enables *continuous tracking* of vehicle locations and therefore of the beams based on the locations.

C. CONNECTED RATE

Not all vehicles will be connected. The connected rate defines the percentage of vehicles with connected devices, whose locations are known to the BS. Lower connected rates might have significant impact on our model since the features need to be properly selected and ordered based on the locations as shown in Section II-D and II-E. With a low connected rate, the vehicle locations might be missing and the features can be misaligned. In this paper, we divide the vehicles into four sets: 1) \mathcal{C} as the connected cars, 2) $\bar{\mathcal{C}}$ as the unconnected cars, 3) connected trucks \mathcal{T} , and 4) unconnected trucks $\bar{\mathcal{T}}$. We assume only the connected cars, i.e., \mathcal{C} , will initiate the beam training requests in the current situational awareness-assisted solution. For the unconnected vehicles, beam training still relies on traditional approaches. To model the different connecting levels, we randomly select trucks and cars as being *connected* based on a Bernoulli distribution with a certain connected rate. Trucks and cars which are not connected will be *invisible* to the BS and the locations will be absent from the features.

IV. GENERALIZATION AND SCALABILITY IN LARGE ANTENNA ARRAYS

Beam selection with situational awareness performs well with a small number of beams in the codebook, using machine learning classification. When the number of beams grows large and therefore a lot of classes are required to be classified, the single-label classification model does not scale well and classification error can be significant due to the complex structure of the learning model and the huge number of hyper-parameters to tune. For example, with a DFT codebook at transmitter and receiver, a 4×4 UPA corresponds to $(4^2)^2 = 256$ beam pairs, while a 16×16 UPA has $(16^2)^2 = 65536$ beam pairs in total. We propose the following approaches to improve the scalability of the situational awareness-aided beam selection and demonstrate its generalization in the large antenna array regime.

In particular, instead of identifying one *single* beam pair based on single-label classification, we aim at relaxing the constraint and *recommending* a small *set* of the beams (K beams) that are *likely* to be optimal. Among the set of the recommended beams, the BS and receiver conduct beam sweeping and the BS selects the beam pair with the highest beam RSRP. We leverage the predicted probability mass function (PMF) of the beams and a *multi-label* classifier to recommend beams.

A. BEAM PROBABILITY DISTRIBUTION

In Section II-A, we explained how random forest classifier can predict the optimal beam pair index given situational awareness. To identify a *set* of likely beams, we leverage the predicted *class probabilities*, i.e., the beam PMF distribution, from the output of random forest classifier. In random forest classification, the classifier makes a *class prediction* for each tree in the random forests. The classifier then *counts* the fraction of trees that *vote* for a certain beam and estimates the beam PMF. The BS then recommends K beam pairs with the *highest* estimated class probabilities. It should be noted that the solution is efficient since it directly leverages the probabilistic output from random forest classification, which can be directly obtained by `predict_proba` function in scikit-learn (sklearn). Optimal beam pair index suffices to establish the dataset, and the model does not require extra feedback from the receiver.

B. MULTI-LABEL CLASSIFICATION

Scalability of the proposed beam selection solution can be achieved by exploiting an extra phase of beam sweeping over the recommended beam pair set. In this section, multi-label classification is considered as an alternative for recommending the beams.

Multi-label classification is a variant of the classification problem where multiple labels are assigned to each instance. In our problem, the labels for the multi-label classification are the top- K beam indexes with the highest beam RSRP. If the optimal beam pair is not included in the recommended set, it is still very likely that at least

TABLE 1. An example of beams in the multi-label dataset. The top-2 beams selected at each geometry are marked by a \times .

	1	2	3	4	labels
SA1	\times	\times			{1, 2}
SA2		\times	\times		{2, 3}
...			
SAn		\times	\times		{3, 4}

TABLE 2. The transformed label for the multi-variate binary classification problem based on the samples in Table 1.

	bc1	bc2	bc3	bc4
SA1	1	1	0	0
SA2	0	1	1	0
...		
SAn	0	0	1	1

one of the *good* beams is in the recommended beam set. In case of a misclassification, the selected beam can still guarantee good performance and will not lead to an outage. We can solve the multi-label classification by formulating an equivalent multi-variate binary classification problem (i.e., the binary relevance method [49]). For example, among the four classes 1, 2, 3, 4 in Table 1, four binary classifiers bc1, bc2, bc3, bc4 will be formulated per class as in Table 2. For each of the sample of one certain class i , if under the current situational awareness (*which is abbreviated as SA in Table 1 and Table 2*), i is among the top- K beams, then the label for the i -th binary classifier is 1, and 0 otherwise. Different from the approach proposed in IV-A which requires the feedback of only the optimal beam pair index, the receiver needs to further feedback the indexes of the top- K beams.

V. PERFORMANCE EVALUATION

In this section, we provide a comprehensive evaluation of the proposed beam selection approach. We focus on the evaluation of two performance metrics: the alignment probability and the achieved throughput ratio. We define c_i as the predicted beam pair index for the i -th data sample in the testing dataset, and s_i as the optimal beam pair index defined in (4). The total number of the samples in the testing dataset is m . In the case of single-label classification, the alignment probability $P_{(1)}$ is equivalent to the definition of the *accuracy* in machine learning classification [17]:

$$P_{(1)} = \frac{1}{m} \sum_{i=1}^m \mathbb{1}(c_i = s_i). \quad (8)$$

For the case when multiple beams are recommended and the recommended beam set for the i -th sample is \mathcal{R}_i , the alignment probability equals the *top- K error* as

$$P_{(K)} = \frac{1}{m} \sum_{i=1}^m \mathbb{1}(s_i \in \mathcal{R}_i). \quad (9)$$

Due to the physical adjacency of beams, especially when the size of the antenna array is large, the difference among the *top* beam RSRPs can be marginal. Hence, we propose to evaluate the throughput achieved with the predicted beam pair as well. The detailed results and discussions are presented in Table 3. In particular, the *reference* throughput is the *ideal* throughput achieved by selecting the optimal beam pair identified by exhaustive beam search. Denoting the beam power of the i -th sample as \mathbf{p}_i , which is defined in (3), we define the *achieved throughput ratio* R_T as

$$R_T = \frac{\sum_{i=1}^m \log_2(1 + \mathbf{p}_i[c_i])}{\sum_{i=1}^m \log_2(1 + \mathbf{p}_i[s_i])}. \quad (10)$$

We start by comparing the performances of beam prediction with different machine learning models. Then we evaluate the alignment probability with different levels of situational awareness by including different numbers of vehicle locations in the features. We examine the effects of several implementation issues on the performance. Last, we demonstrate the performance enhancement with multiple beams recommended.

A. LEARNING MODELS

In Table 3, we compare the alignment probability with different feature encoding approaches. We implement training and testing in disjoint datasets with 80% and 20% out of $\sim 98K$ samples in total. We apply a five-fold cross-validation for the learning. We tune the hyper-parameters for each classifier. The last column in Table 3 shows the *maximum* throughput ratio achieved using the optimal feature encoding per classifier. In the current dataset, we have UPAs of size 4×4 at the transmitter and receiver. From the result, we observe that polar coordinates, especially 3D polar coordinates, perform better than the Cartesian coordinates and the occupancy grids. We also evaluate the classifier performance of RBF-SVM, gradient boosting, random forest, and deep feedforward neural networks. We use sklearn for the training and testing for SVM, gradient boosting, and random forest classification [50]. We implement the deep learning model in Keras [51]. The results show that the random forest outperforms other classifiers, achieving the highest alignment probability of 84.16%.

Another important observation is that the achieved throughput does not *scale* with the alignment probability. Despite the fact that random forest achieves much higher alignment probability compared to other classifiers such as SVM and neural networks, the differences among their achieved throughputs are insignificant. The reason is that the RSRP of the *strongest* several beams are close. The results show that even if the classifier cannot predict the *exact* optimal beam pair index, as long as the selected one is among one of these *strongest* beams, the throughput will not be too bad. The conclusion reveals the fact that alignment probability might not be the *only* important performance metric for evaluation. Even though the model cannot guarantee 100% alignment probability as exhaustive beam search, it could

TABLE 3. Alignment probability and achieved throughput ratio of beam selection on test data with different classifiers.

Alignment prob.(%)	Cartesian	Polar (2D)	Spherical	Grids (2D)	R_T (%)
RBF-SVM	54.14	59.22	58.80	67.66	93.92
Gradient Boosting	75.75	78.84	77.23	76.35	96.04
Deep learning	66.72	68.42	70.41	70.46	85.29
Random forest	83.07	83.95	84.16	76.49	97.66

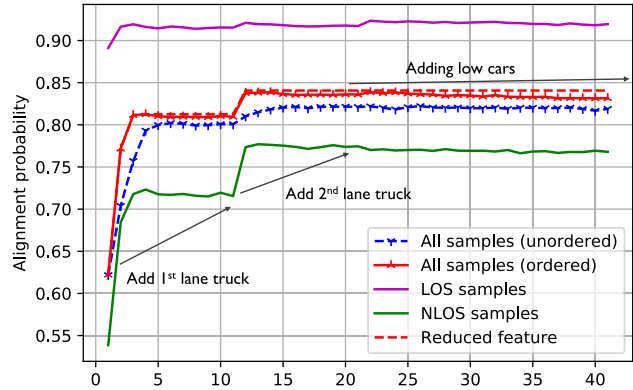


FIGURE 8. Alignment probability with different number of vehicle locations in the features, with LOS samples only, NLOS samples only, the full datasets with/without feature ordering, and the full dataset with a reduced set of features. We start by using only the receiver location in the features. We then add the first-lane trucks, second-lane trucks, first-lane cars, second-lane cars, sequentially in the features, as explained in Section II-E. The red dashed curve is the alignment probability achieved by only including parts of the vehicle locations in the feature, e.g., the receiver and the closest trucks on each lane.

still be accurate enough to identify the good beams. This is important for mmWave vehicular system design, since it is beneficial to *sacrifice some optimality* to largely reduce the overhead.

The result also shows that deep learning does not outperform the random forest classifier. The dataset is highly *unbalanced*, where $\sim 55\%$ of the samples have the *same* class. Compared to deep learning, the random forest classifier is able to handle the imbalance well in our dataset with a relatively small size of data samples. Random forest also generalizes well with *data bagging*, which generates multiple *subsets* of data samples for training from the original dataset using combinations with repetitions [15]. Last, the dimension of the hand-crafted features is relatively small, which makes the random forest an efficient solution to our specific problem and dataset compared to deep learning.

B. EFFECTIVENESS OF SITUATIONAL AWARENESS

In Fig. 8, we evaluate and compare the system performance by incorporating different *levels* of situational awareness in the spherical coordinates. We quantify the levels of situational awareness by the *completeness* of the environment information. To compare, we apply different numbers of *neighboring* vehicles in the features. We evaluate the alignment probability using the LOS dataset, the NLOS dataset, the full dataset with and without the feature ordering, and

the full dataset with a reduced number of features. In the case without feature ordering, the features are concatenated following the procedure in II-E.1. With feature ordering, the locations are ordered based on vehicle's relative distance to the receiver as described in Section II-E.2. For the full dataset, when only the receiver location is included in the features, an alignment probability of around 62% is achieved. After adding the first-lane truck locations to the features, the alignment probability grows to 82%. Similar observations can be obtained by adding the second lane trucks. From the curve, it can be concluded that most of the alignment probability improvement is contributed by the closest trucks' (around only 2-3) locations on each lane.

Furthermore, when small vehicles (cars) are included in the features, the alignment probability remains stable. We come to an important conclusion that reveals the propagation characteristics in mmWave urban vehicular communication. In this paper, the machine learning model captures the relationship between the mmWave channel and the situational awareness that is comprised of the geometry of different vehicles in the urban environment. The negligible improvement of alignment probability by adding more small cars in the features implies that small cars such as sedans have minor impact on mmWave V2I channels. In other words, small cars are not an important source of scattering for mmWave V2I communication in an urban canyon.

We reduce the number of vehicle locations in the features and only keep those vehicle locations that improve the alignment probability. In our dataset, the reduced feature set is: (*receiver location, closest three trucks in the first lane, closest truck in the second lane*). The red dashed curve shows the alignment probability of around 84% when the reduced feature set is used. Also, the *unordered* features give a lower bound for the alignment probability of the *ordered* features as explained in Section II-E.

With different numbers of vehicle locations in the features, the alignment probabilities of the LOS and NLOS datasets exhibit different behaviors. For the LOS dataset, the alignment probability stays constant at around 89% \sim 92%. For the NLOS dataset, the contribution of a higher level of situational awareness becomes prominent. Including the first lane of trucks only, the alignment probability grows from 53% to 72%. More vehicle locations lead to an improvement of NLOS beam prediction accuracy to 78%. The major difference between the LOS and NLOS performance lies in their different reflections and multi-path effects. In LOS samples, the multi-path signature has a dominant LOS path along with

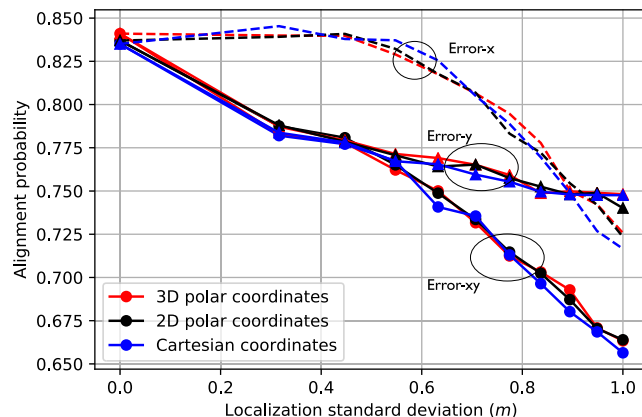


FIGURE 9. Comparison of alignment probability with different levels of localization accuracy, in Cartesian coordinates, 2D polar coordinates and spherical coordinates. Localization errors along and perpendicular to the horizontal direction are evaluated individually. Specifically, the dashed lines represent the case with only the localization error along the horizontal direction. The triangles demonstrate the performance which only includes the location errors perpendicular to lane direction. The circles evaluate the performance which combines the localization errors along both directions.

several weak NLOS paths with reflections. Hence, it is sufficient to directly point the beam towards the receiver, without full knowledge of the neighboring vehicles. For the NLOS receivers, however, reflections become the most important means of establishing a link and are the vital components of the channel. Situational awareness gives the BS the capability to capture the multi-path effect on the surrounding vehicles for NLOS links, which hence enables significant gains in the alignment probability with more vehicle locations included.

C. NOISY FEATURES

In this section, the features include vehicle location inaccuracy as described in Section III. Fig. 9 compares the alignment probability, when different localization inaccuracy modelings are applied. The location inaccuracy of both the x and y coordinates makes a big difference on the prediction accuracy. When the localization error is small, the alignment probability drops significantly with the error of the y coordinate. The sensor might localize the vehicles on a different lane if the error along the y coordinate is large. When the error variance grows large, the localization error on the x coordinate dominates. When the localization error grows large, the prediction accuracy falls below 70%. One limitation of our model is that it heavily relies on the accurate vehicle locations provided by the different sensors. It is promising, however, that sensor fusion of radar, LiDAR and camera can be leveraged from autonomous vehicles to provide more accurate localization and situational awareness knowledge.

Fig. 10 demonstrates how the performance is affected when a longer location reporting interval is applied with vehicle mobility. We summarize the mobility parameters in Table 4. Parameters v_{\max} , v_{\min} represent the upper and lower bounds for the truncated Gaussian distribution of the velocity, while a_{\max} and a_{\min} denote the corresponding bounds for the acceleration rate.

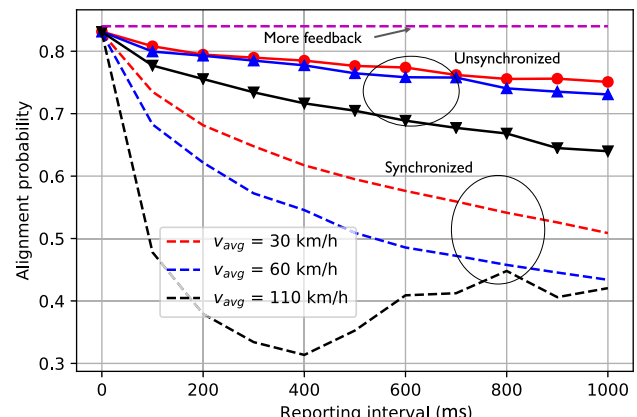


FIGURE 10. Comparison of alignment probability with different vehicle velocities, accelerations and location reporting intervals. Here we consider three different synchronization mechanisms: 1) synchronized feedback, 2) unsynchronized feedback as discussed in Section III-B, and 3) more feedback including velocity and acceleration. Particularly, we assume the acceleration rate remains constant during the 1000 ms we evaluate in the figure. We assume uniformly accelerated rectilinear motion for all vehicles and there are no localization errors modeled in either the training or the testing datasets for fair comparison.

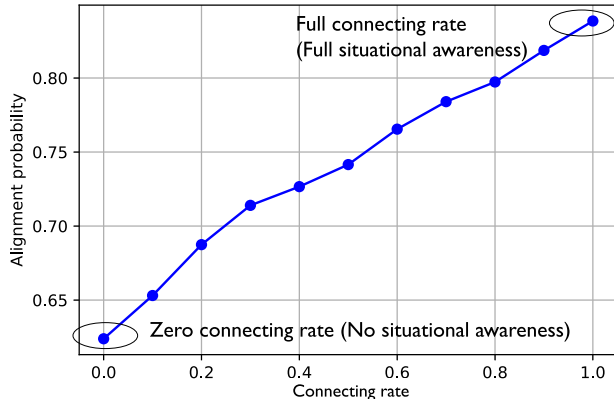
We assume *uniformly accelerated rectilinear motion* for all vehicles, with random velocities and accelerations modeled in Section III-B. For fair comparison, no localization errors are included in the datasets. In the unsynchronized feedback case, the alignment probability degrades with a longer reporting interval. For example, with reporting interval of around 200 ms, the alignment probability drops to around 76% from 84% at $\bar{v} = 110$ km/h. Therefore, if the velocities and accelerations can be fed back to the BS along with the locations, the updated locations can be kept track of and the alignment probability can be guaranteed, with negligible extra feedback overhead required.

In the synchronized feedback case, only the testing dataset has location errors due to vehicle mobility, while the training data is accurate. We can observe that the performance degrades a lot and the learning fails. As shown in the dashed lines, the alignment probability becomes extremely low for a large location reporting interval with a high speed, e.g., $\bar{v} = 110$ km/h. Performance degradation for the synchronized case, however, is expected. Synchronized feedback provides an *error-free* training dataset. The testing dataset, however, is noisy and has a completely *different distribution* from the training data. Hence, the distribution learned from the training data cannot be applied in the testing data for evaluation.

In conclusion, the effect of a longer reporting interval on the performance is significant, especially with high mobility. It is important that more information, including the velocity and acceleration along with the location, is packed and communicated between the vehicles and the BS. The mobility parameters of velocity and acceleration not only avoid the unnecessary noise introduced to the features, they also provide *continuous* tracking of the vehicle locations and therefore enable a *seamless* tracking of the potential beam change. Feedback of vehicle location, velocity and acceleration is

TABLE 4. Mobility parameters for comparing performance of different vehicle location update frequencies.

	\bar{v} m/s	σ_v m/s	v_{\max} m/s	v_{\min} m/s	\bar{a} m/s ²	σ_a m/s ²	a_{\max} m/s ²	a_{\min} m/s ²
Case 1	30	2	30	20	0	1	-1.5	1.5
Case 2	60	4	80	40	0	2	-2	2
Case 3	110	4	120	80	0	2	-2	2

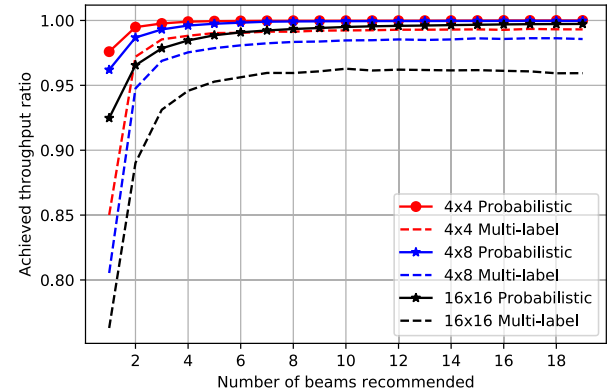
**FIGURE 11.** Comparison of alignment probability with different connected rates in Cartesian coordinates.

sufficient to keep track of the beam, which also eliminates the necessity of frequent exhaustive beam search in case of beam changes.

Fig. 11 plots the alignment probability with different vehicle connected rates. Previous results in Fig. 8 showed that the small cars contribute little to the prediction of the optimal beam pair. Also, since the channels of all small cars are simulated and used for the learning, *disconnecting* some small cars will lead to different numbers of data samples for the learning. Hence, we assume all small cars are connected to the BS. Trucks might be unconnected based on a certain connected rate. Zero connected rate is equivalent to the case without situational awareness, while full connected rate is equivalent to the full situational awareness case as discussed in Section V-B. The alignment probability scales almost linearly with the connected rate. To guarantee prediction accuracy, it may make sense to design an operating mechanism where the beam training can be switched between: (a) the traditional exhaustive beam search approach, and (b) the situational awareness assisted-solution, based on the different vehicle connected rates.

D. GENERALIZATION AND SCALABILITY

To evaluate the scalability of the beam recommendation solutions proposed in Section IV, we compare the achieved throughput ratio R_T with different numbers of beams recommended in Fig. 12, in datasets with various-sized antenna arrays. Even though multi-label classification requires extra feedback from the receiver about the top- K beam pair index, the simple solution based on the estimated beam probability distribution in Section IV-A is accurate and efficient.

**FIGURE 12.** Comparison of achieved throughput ratio R_T with different recommendation solutions and number of antennas deployed. The red curves represent the case with a 4×4 UPA at transmitter and receiver. Blue and black curves represent 4×8 and 16×16 UPAs. The solid lines represent the recommendation based on beam probability distribution. The dashed lines are the results from the recommendation based on multi-label classification.

For the transceivers with UPAs of size 4×4 , the result shows that the estimated probability based solution is able to achieve almost the *ideal* throughput with only *four* beams recommended. It can also be concluded that the proposed solution scales and generalizes well with the large antenna arrays. Even for the case with 16×16 UPAs, by recommending six beams, the throughput loss is *marginal*. It is also observed from Fig. 12 that the gaps among the throughput performance with different antenna arrays are insignificant, due to the physical adjacency of beams for large antenna arrays.

VI. CONCLUSION

In this paper, we proposed a situational awareness-aided beam training solution using machine learning in mmWave V2I communication. Situational awareness provides valuable side information to capture the multi-path and reflection effects in vehicular communication. Exploiting the regularity of the vehicular geometry and moving trajectories, the beam selection was formulated as a classification problem, with features of properly modeled situational awareness. We observed significant improvement of alignment probability when more vehicle locations, i.e., a higher level of situational awareness, are added in the features. We also revealed the fact that the scatterings on small cars are negligible compared to those that happen on the large vehicles such as trucks. Situational awareness was shown to be useful to characterize the physical environment of

vehicular communication in urban canyon. For future work, more detailed situational awareness features of vehicle sizes and exterior shapes can be investigated and generalized in different vehicular contexts, including urban intersection, rural roads, etc.

The proposed beam selection framework is dependent on the availability of accurate localization of vehicles. In practice, however, various factors can lead to inaccurate or incomplete situational awareness. We compared the location inaccuracy introduced by localization error, the limited location updating frequencies from vehicles, and different connected rates of vehicles. The results demonstrated the sensitivity of the proposed model to localization errors. Most of the errors, however, can be corrected either by leveraging advanced localization technologies or by feeding back mobility information, such as velocity and acceleration to the BS. Also, we can shift the *mode* of beam training based on the connected rate, between predicting the beam via the proposed solution and the traditional solution by exhaustive beam search.

The random forest was shown to outperform other classifiers in terms of simplicity, efficiency and accuracy. With a highly unbalanced dataset and the relatively small dimension of features, a random forest classifier was preferred and also *deep* in terms of the large number of trees available in the model. Last, it was shown that with simple statistics obtained from the classification, the scalability of the beam selection approach was achieved by allowing an extra phase of beam sweeping among a small beam search space. Even with a large antenna arrays, e.g., 16×16 UPA, 99% of the throughput can be achieved, which requires search among only six beams.

For future work, temporally-correlated data will be collected through ray tracing through properly modeled vehicle trajectories. Online learning models are one promising approach to test how fast the training accuracy can be improved and how many data samples are needed for satisfactory performance of beam prediction in field implementation. Hybrid beamforming at mmWave is another potential application scenario, which requires joint beam recommendation among multiple RF chains. Last, the situational awareness can be leveraged for full mmWave beam training automation, including the prediction of the beam RSRP, rank of channel, and other relevant channel statistics.

ACKNOWLEDGMENT

This paper was presented at the IEEE Globecom Workshops, 2018 [1].

REFERENCES

- [1] Y. Wang, A. Klautau, M. Ribero, M. Narasimha, and R. W. Heath, Jr., "Mmwave vehicular beam training with situational awareness by machine learning," in *Proc. IEEE Globecom Workshops (GC Wkshps)*, Dec. 2018, pp. 1–6.
- [2] J. Choi, V. Va, N. González-Prelcic, R. Daniels, C. R. Bhat, and R. W. Heath, Jr., "Millimeter-wave vehicular communication to support massive automotive sensing," *IEEE Commun. Mag.*, vol. 54, no. 12, pp. 160–167, Dec. 2016.
- [3] J. Wang, Z. Lan, C.-W. Pyo, T. Baykas, C.-S. Sum, M. A. Rahman, R. Funada, F. Kojima, I. Lakkis, and H. Harada, "Beam codebook based beamforming protocol for multi-Gbps millimeter-wave WPAN systems," in *Proc. IEEE Global Telecommun. Conf.*, Nov./Dec. 2009, pp. 1–6.
- [4] Y. M. Tsang, A. S. Y. Poon, and S. Addepalli, "Coding the beams: Improving beamforming training in mmWave communication system," in *Proc. IEEE Global Telecommun. Conf.*, Dec. 2011, pp. 1–6.
- [5] Z. Xiao, T. He, P. Xia, and X.-G. Xia, "Hierarchical codebook design for beamforming training in millimeter-wave communication," *IEEE Trans. Wireless Commun.*, vol. 15, no. 5, pp. 3380–3392, May 2016.
- [6] N. González-Prelcic, A. Ali, V. Va, and R. W. Heath, Jr., "Millimeter-wave communication with out-of-band information," *IEEE Commun. Mag.*, vol. 55, no. 12, pp. 140–146, Dec. 2017.
- [7] Y. Wang, K. Venugopal, R. W. Heath, Jr., and A. F. Molisch, "MmWave vehicle-to-infrastructure communication: Analysis of urban microcellular networks," *IEEE Trans. Veh. Technol.*, vol. 67, no. 8, pp. 7086–7100, Aug. 2018.
- [8] M. Peng, Y. Li, J. Jiang, J. Li, and C. Wang, "Heterogeneous cloud radio access networks: A new perspective for enhancing spectral and energy efficiencies," *IEEE Wireless Commun.*, vol. 21, no. 6, pp. 126–135, Dec. 2014.
- [9] L. Breiman, "Random forests," *Mach. Learn.*, vol. 45, no. 1, pp. 5–32, 2001.
- [10] V. Svetnik, A. Liaw, C. Tong, J. C. Culberson, R. P. Sheridan, and B. P. Feuston, "Random forest: A classification and regression tool for compound classification and qsar modeling," *J. Chem. Inf. Comput. Sci.*, vol. 43, no. 6, pp. 1947–1958, 2003.
- [11] D. R. Cutler, T. C. Edwards, Jr., K. H. Beard, A. Cutler, K. T. Hess, J. Gibson, and J. J. Lawler, "Random forests for classification in ecology," *Ecology*, vol. 88, no. 11, pp. 2783–2792, Nov. 2007.
- [12] J. Friedman, T. Hastie, and R. Tibshirani, *The Elements of Statistical Learning*, vol. 1. New York, NY, USA: Springer, 2001.
- [13] T. G. Dietterich, "Ensemble learning," in *The Handbook of Brain Theory and Neural Networks*, vol. 2. Cambridge, MA, USA: MIT Press, 2002, pp. 110–125.
- [14] L. Breiman, J. Friedman, C. J. Stone, and R. A. Olshen, *Classification and Regression Trees*. Boca Raton, FL, USA: CRC Press, 1984.
- [15] L. Breiman, "Bagging predictors," *Mach. Learn.*, vol. 24, no. 2, pp. 123–140, 1996.
- [16] Z.-H. Zhou, *Ensemble Methods: Foundations and Algorithms*. Boca Raton, FL, USA: CRC Press, 2012.
- [17] S. B. Kotsiantis, I. Zaharakis, and P. Pintelas, "Supervised machine learning: A review of classification techniques," in *Emerging Artificial Intelligence Applications in Computer Engineering*, vol. 160. 2007, pp. 3–24.
- [18] A. Ali, N. González-Prelcic, and R. W. Heath, Jr., "Millimeter wave beam-selection using out-of-band spatial information," *IEEE Trans. Wireless Commun.*, vol. 17, no. 2, pp. 1038–1052, Feb. 2018.
- [19] A. Asadi and S. Müller, G. H. Sim, A. Klein, and M. Hollick, "FML: Fast machine learning for 5G mmwave vehicular communications," in *Proc. IEEE Conf. Comput. Commun.*, Apr. 2018, pp. 1961–1969.
- [20] A. Alkhateeb, S. Alex, P. Varkey, Y. Li, Q. Qu, and D. Tujkovic, "Deep learning coordinated beamforming for highly-mobile millimeter wave systems," *IEEE Access*, vol. 6, pp. 37328–37348, 2018.
- [21] V. Va, J. Choi, T. Shimizu, G. Bansal, and R. W. Heath, Jr., "Inverse multipath fingerprinting for millimeter wave V2I beam alignment," *IEEE Trans. Veh. Technol.*, vol. 67, no. 5, pp. 4042–4058, May 2018.
- [22] V. Va, T. Shimizu, G. Bansal, and W. R. Heath, Jr., "Position-aided millimeter wave V2I beam alignment: A learning-to-rank approach," in *Proc. IEEE 28th Annu. Int. Symp. Pers., Indoor, Mobile Radio Commun. (PIMRC)*, Oct. 2017, pp. 1–5.
- [23] A. Klautau, P. Batista, N. González-Prelcic, Y. Wang, and R. W. Heath, Jr., "5G MIMO data for machine learning: Application to beam-selection using deep learning," in *Proc. Inf. Theory Appl. Workshop (ITA)*, Feb. 2016, pp. 1–6.
- [24] Y. Wang, M. Narasimha, and R. W. Heath, Jr., "MmWave beam prediction with situational awareness: A machine learning approach," in *Proc. IEEE 19th Int. Workshop Signal Process. Adv. Wireless Commun. (SPAWC)*, Jun. 2015, pp. 1–5.
- [25] H. Zhao, R. Mayzus, S. Sun, M. Samimi, J. K. Schulz, Y. Azar, K. Wang, G. N. Wong, F. Gutierrez, Jr., and T. S. Rappaport, "28 GHz millimeter wave cellular communication measurements for reflection and penetration loss in and around buildings in New York city," in *Proc. IEEE Int. Conf. Commun. (ICC)*, Jun. 2013, pp. 5163–5167.

- [26] J.-J. Park, J. Lee, J. Liang, K.-W. Kim, K.-C. Lee, and M.-D. Kim, "Millimeter wave vehicular blockage characteristics based on 28 GHz measurements," in *Proc. IEEE 86th Veh. Technol. Conf. (VTC-Fall)*, Sep. 2017, pp. 1–5.
- [27] V. Va, T. Shimizu, G. Bansal, and R. W. Heath, Jr., "Online learning for position-aided millimeter wave beam training," *IEEE Access*, vol. 7, pp. 30507–30526, May 2019.
- [28] A. S. Glassner, *An Introduction to Ray Tracing*. Amsterdam, The Netherlands: Elsevier, 1989.
- [29] V. Degli-Esposti, F. Fuschini, E. M. Vitucci, M. Barbiroli, M. Zoli, L. Tian, X. Yin, D. A. Dupleich, and R. Müller, C. Schneider, "Ray-tracing-based mm-Wave beamforming assessment," *IEEE Access*, vol. 2, pp. 1314–1325, 2014.
- [30] S. Hur, S. Baek, B. Kim, J. Park, A. F. Molisch, K. Haneda, and M. Peter, "28 GHz channel modeling using 3D ray-tracing in urban environments," in *Proc. 9th Eur. Conf. Antennas Propag. (EuCAP)*, Apr. 2015, pp. 1–5.
- [31] K. Haneda, L. Tian, H. Asplund, J. Li, Y. Wang, D. Steer, C. Li, T. Balercia, S. Lee, and Y. Kim, "Indoor 5G 3GPP-like channel models for office and shopping mall environments," in *Proc. IEEE Int. Conf. Commun. Workshops (ICC)*, May 2016, pp. 694–699.
- [32] S. Y. Seidel and T. S. Rappaport, "Site-specific propagation prediction for wireless in-building personal communication system design," *IEEE Trans. Veh. Technol.*, vol. 43, no. 4, pp. 879–891, Nov. 1994.
- [33] *Wireless Insite*. Accessed: 2018. [Online]. Available: <https://www.remcom.com/wireless-insite-em-propagation-software/>
- [34] W. B. Powell, "A stochastic model of the dynamic vehicle allocation problem," *Transp. Sci.*, vol. 20, no. 2, pp. 117–129, May 1986.
- [35] F. Ye and Y. Zhang, "Vehicle type-specific headway analysis using freeway traffic data," *Transp. Res. Rec. J. Transp. Res. Board*, vol. 2124, no. 1, pp. 222–230, Dec. 2009.
- [36] Y. Wang. (2019). *Situational Awareness for mmWave Beam Training*. [Online]. Available: <https://github.com/yuyangwang/SituationalAwareBeamAlignment>
- [37] T. S. Rappaport, R. W. Heath, Jr., R. C. Daniels, and J. N. Murdock, *Millimeter Wave Wireless Communications*. London, U.K.: Pearson, 2014.
- [38] Y.-H. Nam, B. L. Ng, K. Sayana, Y. Li, J. Zhang, Y. Kim, and J. Lee, "Full-dimension MIMO (FD-MIMO) for next generation cellular technology," *IEEE Commun. Mag.*, vol. 51, no. 6, pp. 172–179, Jun. 2013.
- [39] J. Ngiam, A. Khosla, M. Kim, J. Nam, H. Lee, and A. Y. Ng, "Multimodal deep learning," in *Proc. 28th Int. Conf. Mach. Learn. (ICML)*, 2011, pp. 689–696.
- [40] M. Modsching, R. Kramer, and K. T. Hagen, "Field trial on GPS accuracy in a medium size city: The influence of built-up," in *Proc. 3rd Workshop Positioning, Navigat. Commun.*, Mar. 2006, pp. 209–218.
- [41] W. Wu, W. Jin, and L. Shen, "Mixed platoon flow dispersion model based on speed-truncated Gaussian mixture distribution," *J. Appl. Math.*, vol. 2013, May 2013, Art. no. 480965.
- [42] Y. Wang, W. Dong, L. Zhang, D. Chin, M. Papageorgiou, G. Rose, and W. Young, "Speed modeling and travel time estimation based on truncated normal and lognormal distributions," *Transp. Res. Rec. J. Transp. Res. Board*, vol. 2315, no. 1, pp. 66–72, Jan. 2012.
- [43] Y. Zhang, G. W. Gantt, M. J. Rychlinski, R. M. Edwards, J. J. Correia, and C. E. Wolf, "Connected vehicle diagnostics and prognostics, concept, and initial practice," *IEEE Trans. Rel.*, vol. 58, no. 2, pp. 286–294, Jun. 2009.
- [44] D. Jiang, V. Taliwal, A. Meier, W. Hoffelder, and R. Herrtwich, "Design of 5.9 GHz DSRC-based vehicular safety communication," *IEEE Wireless Commun.*, vol. 13, no. 5, pp. 36–43, Oct. 2006.
- [45] J. B. Kenney, "Dedicated short-range communications (DSRC) standards in the United States," *Proc. IEEE*, vol. 99, no. 7, pp. 1162–1182, Jul. 2011.
- [46] *Vehicle Based Data and Availability*. Accessed: 2012. [Online]. Available: https://www.its.dot.gov/itspac/october2012/PDF/data_availability.pdf
- [47] H. Rakha, M. Snare, and F. Dion, "Vehicle dynamics model for estimating maximum light-duty vehicle acceleration levels," *Transp. Res. Rec. J. Transp. Res. Board*, vol. 1883, no. 1, pp. 40–49, 2004.
- [48] R. Akçelik and M. Besley, "Acceleration and deceleration models," in *Proc. Conf. Austral. Institutes Transp. Res.(CAITR)*, Dec. 2001, p. 12.
- [49] G. Tsoumakas and I. Vlahavas, "Random k-Labelsets: An ensemble method for multilabel classification," in *Proc. Eur. Conf. Mach. Learn.* Berlin, Germany: Springer, 2007, pp. 406–417.
- [50] F. Pedregosa, G. Varoquaux, A. Gramfort, V. Michel, B. Thirion, O. Grisel, M. Blondel, P. Prettenhofer, R. Weiss, V. Dubourg, J. Vanderplas, A. Passos, D. Cournapeau, M. Brucher, M. Perrot, and É. Duchesnay, "Scikit-learn: Machine learning in python," *J. Mach. Learn. Res.*, vol. 12, pp. 2825–2830, Oct. 2011.
- [51] F. Chollet. (2015). *Keras*. [Online]. Available: <https://keras.io>



YUYANG WANG (S'17) received the B.S. degree in electrical engineering from Southeast University, Nanjing, China, in 2015, and the M.S.E. degree in electrical engineering from The University of Texas at Austin, Austin, TX, USA, in 2017, where she is currently pursuing the Ph.D. degree with the Wireless Networking and Communications Group, Department of Electrical and Computer Engineering. Her research interests include millimeter-wave (mmWave) vehicular communication and the emerging intersection areas of machine learning, and mmWave V2X. She was the Outstanding Winner of the American Mathematical Contest in Modeling, in 2014, and was recognized as the Outstanding Graduate Student from Southeast University, in 2015. She was an Exemplary Reviewer of the IEEE WIRELESS COMMUNICATIONS LETTERS, in 2015.



ALDEBARO KLAUTAU (S'92–M'97–SM'08) received the Ph.D. degree from the University of California at San Diego, San Diego, CA, USA, in 2003. In 1995, he was a Faculty Member with the Federal University of Santa Catarina, Florianópolis, Brazil. Since 1996, he has been with the Federal University of Pará (UFPA), Belém, Brazil, affiliated with the Computer Science (PPGCC) and Electrical Engineering (PPGEE) Graduate Programs. At UFPA, he is currently with the ITU-T TIES Focal Point and directs the Signal Processing (LaPS) and the Embedded Systems (LASSE) research groups. His research interests include signal processing and machine learning applied to telecommunications. He is also a Researcher of the Brazilian National Council of Scientific and Technological Development (CNPq).



MÓNICA RIBERO (S'17) received the B.S. degree in mathematics from the Universidad de Los Andes, Bogotá, Colombia, in 2015. She is currently pursuing the Ph.D. degree in electrical engineering with the Wireless Networking and Communication Group, Department of Electrical and Computer Engineering, The University of Texas at Austin, Austin, TX, USA. She has held internship positions with Bell Laboratories, Holmdel, NJ, USA. She has worked in machine learning applications to wireless communications and propagation. Her research interests include adapting machine learning models, and training algorithms to distributed and federated learning, particularly to setting where resources are limited by privacy and communication rates. She received the Best Summer Intern Presentation Award from Bell Laboratories.



ANTHONY C. K. SOONG (S'88–M'91–SM'02–F'14) received the B.Sc. degree in animal physiology and physics from the University of Calgary, Calgary, AB, Canada, and the B.Sc. degree in electrical engineering, the M.Sc. degree in biomedical physics, and the Ph.D. degree in electrical and computer engineering from the University of Alberta, Edmonton, AB, Canada. He is currently the Chief Scientist for wireless research and standards at Futurewei Technologies Co. Ltd., Plano, TX, USA. Prior to joining Futurewei, he was with the Systems Group, Ericsson, Inc., and Qualcomm, Inc. He has published numerous scientific papers and has over 80 patents granted or pending. He served as the Chair for 3GPP2 TSG-C NTAH (the next generation radio access network technology development group), from 2007 to 2009, and the Vice Chair for 3GPP2 TSG-C WG3 (the physical layer development group for CDMA 2000), from 2006 to 2011. He was a co-recipient of the 2013 IEEE Signal Processing Society Best Paper Award.



ROBERT W. HEATH, JR. (S'96–M'01–SM'06–F'11) received the B.S. and M.S. degrees from the University of Virginia, Charlottesville, VA, USA, in 1996 and 1997, respectively, and the Ph.D. degree from Stanford University, Stanford, CA, USA, in 2002, all in electrical engineering. From 1998 to 2001, he was a Senior Member of the Technical Staff and then a Senior Consultant with Iospan Wireless, Inc., San Jose, CA, USA, where he worked on the design and implementation of the physical and link layers of the first commercial multi-input-multi-output (MIMO)-OFDM communication system. Since 2002, he has been with the Department of Electrical and Computer Engineering, The University of Texas at Austin, Austin, TX, USA, where he is a Cullen Trust for Higher Education Endowed Professor and a member of the Wireless Networking and Communications Group. He is also the President and the CEO of MIMO Wireless Inc. He has authored the books, *Introduction to Wireless Digital Communication* (Prentice Hall, 2017) and *Digital Wireless Communication: Physical Layer Exploration Lab Using the NI USRP* (National Technology and Science Press, 2012), and has coauthored the book, *Millimeter Wave Wireless Communications* (Prentice Hall, 2014). He has been a coauthor of 16 award winning conference and journal papers, including the 2010 and 2013 EURASIP Journal on Wireless Communications and Networking Best Paper Awards, the 2012 Signal Processing Magazine Best Paper Award, the 2013 Signal Processing Society Best Paper Award, the 2014 EURASIP Journal on Advances in Signal Processing Best Paper Award, the 2014 Journal of Communications and Networks Best Paper Award, the 2016 IEEE Communications Society Fred W. Ellersick Prize, the 2016 IEEE Communications and Information Theory Societies Joint Paper Award, and the 2017 Marconi Prize Paper Award. He received the 2017 EURASIP Technical Achievement Award. He was a Distinguished Lecturer with the IEEE Signal Processing Society. He is an ISI Highly Cited Researcher. In 2017, he was selected as a Fellow of the National Academy of Inventors. He is also an elected member of the Board of Governors for the IEEE Signal Processing Society, a licensed Amateur Radio Operator, a Private Pilot, and a registered Professional Engineer in Texas.